IEEE Access
Multidisciplinary | Rapid Review | Open Access Journal

Received August 28, 2017, accepted September 25, 2017, date of publication September 29, 2017,
date of current version October 25, 2017.

Digital Object Identifier 10.1109/ACCESS.2017.2757932

Computational Efficient Two-Dimension DOA Estimation for Incoherently Distributed Noncircular Sources With Automatic Pairing

ZHENGLIANG DAI, BIN BA, WEIJIA CUI, AND YOUMING SUN, (Student Member, IEEE)
National Digital Switching System Engineering and Technological Research Center, Zhengzhou 450000, China

Corresponding author: Zhengliang Dai (xinxidailiang@outlook.com)

This work was supported by the National Natural Science Foundation of China under Grant 61401513.

ABSTRACT In this paper, the problem of two-dimensional (2-D) direction-of-arrival (DOA) estimation for incoherently distributed (ID) noncircular sources is addressed. A low-complexity estimator with automatic pairing in the three-parallel uniform linear arrays (ULAs) is proposed. First, the signal non-circularity is applied to establish an extended generalized array manifold (GAM) model based on one-order Taylor series approximation. Resorting to such model, the generalized rotational invariance relationships are identified among the extended GAM matrices of the three ULAs. Thereafter, a modified propagator method is utilized to estimate the central elevation and azimuth DOAs. Without any spectrum searching, estimation or eigenvalue decomposition of the sample covariance matrix, the proposed approach is capable of considerably reducing the calculation cost in comparison with the existing methods. In addition, it can automatically pair the estimated central azimuth and central elevation DOAs. We also derive the Cramer-Rao lower bound regarding the 2-D DOA estimation of the ID noncircular source and conduct the computational complexity analysis. Numerical results demonstrate that the proposed method achieves better estimation performance than the existing methods. Furthermore, it can be applied in the multi-source scenario where different sources may have different angular distribution shapes.

INDEX TERMS Array signal processing, two-dimensional (2-D) direction-of-arrival (DOA), incoherently distributed (ID) sources, noncircular sources, Cramer-Rao lower bound.

I. INTRODUCTION

Traditional direction-finding techniques have generally been developed for the far-field point source model, where the signals are assumed for travelling along a single path to the antenna array [1]–[4]. However, in applications such as wireless communications, passive radars and underwater acoustics, the effect of angular spread cannot always be ignored owing to the multipath phenomena [5], [6]. In this case, a distributed source model would be more appropriate. In general, distributed sources have been classified as coherently distributed (CD) sources and incoherently distributed (ID) sources, which pose to be suitable for slowly time-varying and rapidly time-varying channels, respectively [7]. In this paper, we concentrate on the central DOA estimation of ID sources.

Several angular parameter estimation techniques for ID sources have been developed, such as dispersed signal parametric estimation (DISPARE) algorithm [8], total least square estimation parameter via rotational invariance technique (TLS-ESPRIT) algorithm [9], maximum likelihood (ML) algorithm [10], [11], and covariance matching estimator (COMET) algorithm [12], [13]. In these techniques, signal sources are constructed by using the one-dimensional (1-D) ID source model, where the impinging signal is assumed to be in the same plane with the receiving array. However, in actual three-dimensional space, the impinging signal is not generally in the same plane with the receiving array, which should be modeled as the two-dimensional (2-D) ID sources. Despite the fact that most of the approaches above are proposed for 1-D scenarios, there are some that can be extended to 2-D scenarios [10]–[14], which can achieve optimal or near optimal performance. However, since a 2-D ID source includes four angular parameters: the central azimuth DOA, azimuth angular spread, central elevation DOA and

elevation angular spread, these conventional optimum methods in [10]–[14] all suffer from heavy computational burden due to multi-dimensional spectrum searching.

The high computational complexity is the main problem in respect to the 2-D localization of ID sources. To cope with this challenge, several low-complexity DOA estimation techniques have been proposed through the introduction of approximate source models. Specifically, the authors in [15] considered a pair of uniform circular arrays (UCAs), meanwhile decoupled the 2-D nominal DOAs by Taylor series approximation. Then the central elevation DOA estimates are obtained by using TLS-ESPRIT. Afterwards, by using the estimated elevation DOAs, a generalized multiple signal classification (GMUSIC) method was proposed to estimate the central azimuth DOA, which asked for only 1-D search. In [16], with the aid of two parallel ULAs, a low-complexity 2-D DOA estimation algorithm without multi-dimensional searches was proposed for ID sources as well. Similarly with [15], the central elevation DOA estimates are obtained based on the approximate rotational invariance relationship between two ULAs. Instead of the GMUSIC, a capon method is applied to estimate the central azimuth DOA. Although avoiding multi-dimensional searches, the methods proposed in [15] and [16] both need 1-D search and thus their computational complexities are still quite high. In order to avoid spectrum searching, the literature [17] proposed an ESPRIT-based approach for the 2-D DOA estimation of multiple ID sources employing a large uniform rectangular array. Making use of the linear relations among the array response matrices of different sub-arrays, the central elevation and azimuth DOAs can both be estimated without any spectral searching. Nonetheless, this approach still employs either eigenvalue decomposition (EVD) or singular value decomposition (SVD), which are computationally extensive and time consuming, particularly as the number of antenna array elements is much larger than the number of incident signals. Moreover, the additional parameter pairing procedure is required, which may lead to pairing errors and deteriorate the angle estimation performance.

All the aforementioned techniques focus on the complex circular signal situation. However, in some practical scenarios such as mobile communications, the complex noncircular signals are widely used. Examples of such signals include binary phase shift keying (BPSK), multiple amplitude shift keying (MASK) and so on [18]. Noncircular signals can enlarge the array aperture without adding extra antennas, which significantly improves the performance of angle estimation [19], [20]. By exploiting the signal non-circularity, some effective methods have been developed for the angle parameter estimation of distributed sources [21]–[24]. In particular, the literature [23] proposed an estimator for the 1-D ID noncircular sources based on the cross-correlation matrix. In [24], a new off-grid DOA estimation method based on a parametric sparse representation model was addressed for the 1-D ID noncircular sources. However, the methods of [23] and [24] are both concerned on the 1-D ID noncircular sources. To the best of our knowledge, using signal noncircularity for the parameter estimation of 2-D ID sources has not been reported.

TABLE 1. Key notations used in this paper.

Notations	Explanation
$(\cdot)^*$, $(\cdot)^T$, $(\cdot)^H$	Conjugate, transpose and conjugate transpose
$E\{\cdot\}$	Statistical expectation operator
$\delta(\cdot)$	Kronecker delta function
$\mathrm{diag}(\cdot)$	Diagonalization operation
$(\cdot)^+$	Pseudoinverse operation
$\mathbf{I}_p$	$p \times p$ identity matrix
$\mathbf{0}_{p\times q}$	$p \times q$ zero matrix
$[\cdot]_{p,q}$	(p, q)-th entry of a matrix
$[\cdot]_p$	p-th element of a vector
$tr(\cdot)$	Matrix trace
$\odot$	Schur-Hadamard product
$\mathrm{angle}(\cdot)$	Phase acquired operation
$\lvert\cdot\rvert$	Amplitude acquired operation

In this paper, a computational efficient algorithm is proposed for the 2-D central DOA estimation of ID noncircular sources in the three-parallel ULAs. Applying the extended generalized array manifold (GAM) model based on Taylor series approximation, we first establish the generalized rotational invariance relationships among the extended GAM matrices of three ULAs. Then the central azimuth and elevation DOAs are estimated by a modified propagator method (PM). More specifically, the main contributions of this paper are summarized as follows.

(1) An extended GAM model is established based on Taylor series approximation, which exploits signal noncircularity to increase the number of detectable directions and improve the estimation accuracy.
(2) A modified PM based on the extended GAM model is proposed to estimate the 2-D central DOA, which does not require any spectrum searching, estimation or eigenvalue decomposition of sample covariance matrix. As a result, it requires a significantly lower computational complexity than the existing algorithms. In addition, the estimated central azimuth and elevation DOAs can be paired automatically.
(3) The Cramer-Rao lower bound of the proposed estimator is derived regarding the 2-D DOA estimation of ID noncircular source.

The paper is organized as follows. In Section II, the system model and the major assumptions are given. In Section III, we present the extended GAM model and the proposed algorithm. The analysis of the proposed algorithm is provided in Section IV. Finally, the computer simulation results that serve to validate the theoretical results are presented in Section V.

Note that we list the key notations throughout the paper in Table 1 for conciseness.

II. SYSTEM MODEL

As illustrated in Fig. 1, the array geometry consists of three parallel ULAs X, Y and Z. Each ULA is composed of

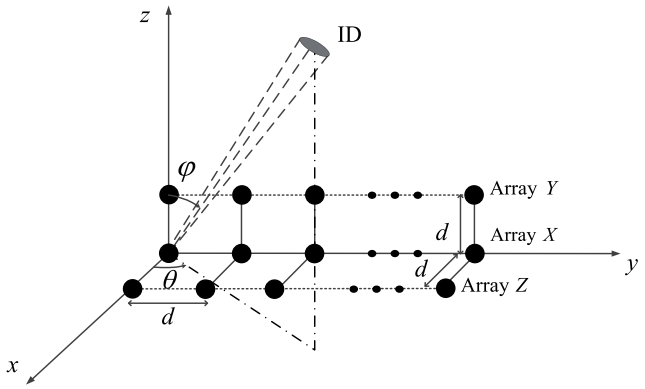

FIGURE 1. The array configuration of three-parallel ULAs.

M omnidirectional sensor elements. The distance of adjacent sensors in each ULA is d, and the distance between adjacent ULAs is also d. We consider K narrowband far-field ID noncircular sources impinging on the array. The output signal vectors of the three sub-arrays X, Y and Z can be expressed as [15]–[17]

$$\boldsymbol{w}_\varepsilon(t) = \sum_{k=1}^{K} s_k(t) \sum_{l=1}^{L_k} \gamma_{k,l}(t)\boldsymbol{a}_\varepsilon(\theta_{k,l}(t), \varphi_{k,l}(t)) + \boldsymbol{n}_\varepsilon(t), \varepsilon \in \{x, y, z\}, \quad (1)$$

where $\boldsymbol{w}_\varepsilon\ (t)(\varepsilon \in \{x, y, z\})$ are the output signal vectors of the three sub-array X, Y and Z, respectively; $t = 1, 2, \ldots, T$ is the sampling time, and T is the total number of snapshots; $s_k\ (t)$ is the complex-valued signal from the k-th source, and L_k is the number of multipath of the k-th source; $\gamma_{k,l}(t)$, $\theta_{k,l}(t)$ and $\varphi_{k,l}(t)$ are the path gain, the azimuth DOA and the elevation DOA of the l-th path from the k-th source, respectively. $\boldsymbol{n}_\varepsilon\ (t)(\varepsilon \in \{x, y, z\})$ are Gaussian white noise vectors with zeros mean and variance σ^2 of the three sub-arrays; additionally, $\boldsymbol{a}_\varepsilon\ (\theta_{k,l}, \varphi_{k,l})(\varepsilon \in \{x, y, z\})$ are the array steering vectors of three sub-arrays X, Y and Z at 2-D DOA $(\theta_{k,l}, \varphi_{k,l})$ having the forms

$$\boldsymbol{a}_x(\theta_{k,l}, \varphi_{k,l}) = [1, e^{-j2\pi(d/\lambda)\sin\theta_{k,l}\sin\varphi_{k,l}}, \cdots, e^{-j2\pi(d/\lambda)(M-1)\sin\theta\sin\varphi}], \quad (2)$$

$$\boldsymbol{a}_y(\theta_{k,l}, \varphi_{k,l}) = \boldsymbol{a}_x(\theta_{k,l}, \varphi_{k,l})g(\varphi_{k,l}), \quad (3)$$

$$\boldsymbol{a}_z(\theta_{k,l}, \varphi_{k,l}) = \boldsymbol{a}_x(\theta_{k,l}, \varphi_{k,l})h(\theta_{k,l}, \varphi_{k,l}), \quad (4)$$

where $g(\varphi_{k,l}) = e^{-j2\pi\ (d/\lambda)\cos\varphi_{k,l}}$, $h(\theta_{k,l}, \varphi_{k,l}) = e^{-j2\pi\ (d/\lambda)\sin\varphi_{k,l}\cos\theta_{k,l}}$, and λ is the signal wavelength.

We can represent $\theta_{k,l}(t)$ and $\varphi_{k,l}(t)$ as

$$\theta_{k,l}(t) = \theta_k + \tilde{\theta}_{k,l}(t), \quad (5)$$

$$\varphi_{k,l}(t) = \varphi_k + \tilde{\varphi}_{k,l}(t), \quad (6)$$

where θ_k and φ_k are the central azimuth DOA and central elevation DOA of the k-th source; $\tilde{\theta}_{k,l}(t)$ and $\tilde{\varphi}_{k,l}(t)$ are the corresponding small random angular deviations, which are assumed as real-valued zero-mean random variables with variances $\sigma^2_{\theta_k}$ and $\sigma^2_{\varphi_k}$, respectively. This small angular spread assumption is reasonable. For example, in suburban and rural environments, a high placement of base station can provide small angular spreads up to 10° [25].

In this paper, the following initial assumptions are considered.

- The path gains $\gamma_{k,l}(t)$ $(k = 1, 2, \cdots, K;\ l = 1, 2, \cdots, L_k;\ t = 1, 2, \cdots, T)$ are assumed as temporally independent and identically distributed (i.i.d.) Gaussian random variables with covariance [16], [17]

$$E\{\gamma_{k,l}(t)\gamma^*_{\tilde{k},\tilde{l}}(\tilde{t})\} = \frac{\sigma^2_{\gamma_k}}{L_k}\delta(k-\tilde{k})\delta(l-\tilde{l})\delta(t-\tilde{t}). \quad (7)$$

- The angular spreads, $\varsigma_1 \triangleq \tilde{\theta}_{k,l}(t)$ and $\varsigma_2 \triangleq \tilde{\varphi}_{k,l}(t)$ $(k = 1, 2, \cdots, K;\ l = 1, 2, \cdots, L_k;\ t = 1, 2, \cdots, T)$, are also temporally i.i.d. real-valued zero-mean random variables with probability density function $p_k\ (\varsigma_1, \varsigma_2; \sigma_{\theta_k}, \sigma_{\varphi_k})$. Moreover, $p_k\ (\varsigma_1, \varsigma_2; \sigma_{\theta_k}, \sigma_{\varphi_k})$ is generally assumed as a symmetric function in ς_1 and ς_2. Now we consider two typical distributions of $p_i\ (\varsigma_1, \varsigma_2; \sigma_{\theta_i}, \sigma_{\varphi_i})$ [15]. They are uniform shape

$$p_k\ (\varsigma_1, \varsigma_2; \sigma_{\theta_k}, \sigma_{\varphi_k}) = \begin{cases} \dfrac{1}{2\sqrt{3}\sigma_{\theta_k}}, & |\varsigma_1| < \sqrt{3}\sigma_{\theta_k} \\ \dfrac{1}{2\sqrt{3}\sigma_{\varphi_k}}, & |\varsigma_2| < \sqrt{3}\sigma_{\varphi_k}, \\ 0, & \text{otherwise} \end{cases} \quad (8)$$

and Gaussian shape

$$p_k(\varsigma_1, \varsigma_2; \sigma_{\theta_k}, \sigma_{\varphi_k}) = \frac{1}{2\pi\sigma_{\theta_k}\sigma_{\varphi_k}} e^{-1/2(\varsigma_1^2/\sigma^2_{\theta_k} + \varsigma_2^2/\sigma^2_{\varphi_k})}. \quad (9)$$

III. ANGLE ESTIMATION ALGORITHM

A. EXTENDED GAM MODELING BASED ON NONCIRCULAR SOURCE

With the first order Taylor series expansion of $\boldsymbol{a}_\varepsilon\ (\theta_{k,l}, \varphi_{k,l})(\varepsilon \in \{x, y, z\})$ around $(\theta_{k,l}, \varphi_{k,l}) = (\theta_k, \varphi_k)$ in the case of small angular spreads, it can be approximated as

$$\boldsymbol{a}_\varepsilon(\theta_{k,l}, \varphi_{k,l}) \approx \boldsymbol{a}_\varepsilon(\theta_k, \varphi_k) + \boldsymbol{a}'_{\varepsilon\theta}(\theta_k, \varphi_k)(\theta_{k,l} - \theta_k) + \boldsymbol{a}'_{\varepsilon\varphi}(\theta_k, \varphi_k)(\varphi_{k,l} - \varphi_k), \quad \varepsilon \in \{x, y, z\}, \quad (10)$$

where $\boldsymbol{a}'_{\varepsilon\theta}(\theta_k, \varphi_k)$ and $\boldsymbol{a}'_{\varepsilon\varphi}(\theta_k, \varphi_k)$ are the first-order partial derivatives of $\boldsymbol{a}_\varepsilon\ (\theta, \varphi)$ around $\theta = \theta_k$ and $\varphi = \varphi_k$, respectively.

Substitute (10) into (1), and $\boldsymbol{w}_\varepsilon(t)(\varepsilon \in \{x, y, z\})$ can approximately be written as

$$\boldsymbol{w}_\varepsilon(t) \approx \sum_{k=1}^{K} \left(\boldsymbol{a}_\varepsilon(\theta_k, \varphi_k)\alpha_{0k} + \boldsymbol{a}'_{\varepsilon\theta}(\theta_k, \varphi_k)\alpha_{\theta k} + \boldsymbol{a}'_{\varepsilon\varphi}(\theta_k, \varphi_k)\alpha_{\varphi k}\right) + \boldsymbol{n}_\varepsilon(t), \varepsilon \in \{x, y, z\}, \quad (11)$$

where the random variables α_{0k}, $\alpha_{\theta k}$ and $\alpha_{\varphi k}$ are defined as

$$\begin{aligned}\alpha_{0k} &= s_k(t)\sum_{l=1}^{L_k}\gamma_{k,l}(t),\\ \alpha_{\theta k} &= s_k(t)\sum_{l=1}^{L_k}\gamma_{k,l}(t)(\theta_{k,l}-\theta_k),\\ \alpha_{\varphi k} &= s_k(t)\sum_{l=1}^{L_k}\gamma_{k,l}(t)(\varphi_{k,l}-\varphi_k).\end{aligned} \tag{12}$$

Therefore, we can reformulate (11) into the GAM model as

$$\boldsymbol{w}_\varepsilon(t) = \bar{\boldsymbol{A}}_\varepsilon \bar{\boldsymbol{s}}(t) + \boldsymbol{n}_\varepsilon(t), \quad \varepsilon \in \{x, y, z\}, \tag{13}$$

where

$$\begin{aligned}\bar{\boldsymbol{A}}_\varepsilon = [&\boldsymbol{a}_\varepsilon(\theta_1,\varphi_1), \boldsymbol{a}_\varepsilon(\theta_2,\varphi_2), \cdots, \boldsymbol{a}_\varepsilon(\theta_K,\varphi_K),\\ &\boldsymbol{a}'_{\varepsilon\theta}(\theta_1,\varphi_1), \boldsymbol{a}'_{\varepsilon\theta}(\theta_2,\varphi_2), \cdots, \boldsymbol{a}'_{\varepsilon\theta}(\theta_K,\varphi_K),\\ &\boldsymbol{a}'_{\varepsilon\varphi}(\theta_1,\varphi_1), \boldsymbol{a}'_{\varepsilon\varphi}(\theta_2,\varphi_2), \cdots, \boldsymbol{a}'_{\varepsilon\varphi}(\theta_K,\varphi_K)]\\ &\in \mathbb{C}^{M\times 3K},\end{aligned} \tag{14}$$

$$\begin{aligned}\bar{\boldsymbol{s}}(t) = [&\alpha_{01}, \alpha_{02}, \cdots, \alpha_{0K}, \alpha_{\theta 1}, \alpha_{\theta 2}, \cdots,\\ &\alpha_{\theta K}, \alpha_{\varphi 1}, \alpha_{\varphi 2}, \cdots, \alpha_{\varphi K}]^T \in \mathbb{C}^{3K\times 1}.\end{aligned} \tag{15}$$

It's worth noting that the GAM matrices $\bar{\boldsymbol{A}}_\varepsilon$ ($\varepsilon \in \{x, y, z\}$) depend only on the central DOAs.

From (3), it can be found that the array steering vectors of sub-arrays X and Y are linearly related, and we can further obtain

$$\boldsymbol{a}'_{y\theta}(\theta_k,\varphi_k) = \boldsymbol{a}'_{x\theta}(\theta_k,\varphi_k)g(\varphi_k), \tag{16}$$

$$\boldsymbol{a}'_{y\varphi}(\theta_k,\varphi_k) = \boldsymbol{a}'_{x\varphi}(\theta_k,\varphi_k)g(\varphi_k) + \boldsymbol{a}_x(\theta_k,\varphi_k)g'(\varphi_k), \tag{17}$$

where $g'(\varphi_k)$ are the first-order partial derivatives of $g(\varphi)$ around $\varphi = \varphi_k$.

According to (3), (13), (16) and (17), we can establish the following generalized rotational invariance relationship as

$$\bar{\boldsymbol{A}}_y = \bar{\boldsymbol{A}}_x \boldsymbol{\Phi}, \tag{18}$$

where

$$\boldsymbol{\Phi} = \begin{bmatrix}\boldsymbol{\Lambda}_{Y1} & \boldsymbol{0}_{K\times K} & \boldsymbol{\Lambda}_{Y2}\\ \boldsymbol{0}_{K\times K} & \boldsymbol{\Lambda}_{Y1} & \boldsymbol{0}_{K\times K}\\ \boldsymbol{0}_{K\times K} & \boldsymbol{0}_{K\times K} & \boldsymbol{\Lambda}_{Y1}\end{bmatrix} \in \mathbb{C}^{3K\times 3K}, \tag{19}$$

in which,

$$\boldsymbol{\Lambda}_{Y1} = diag(g(\varphi_1), g(\varphi_2), \cdots, g(\varphi_K)) \in \mathbb{C}^{K\times K}, \tag{20}$$

$$\boldsymbol{\Lambda}_{Y2} = diag(g'(\varphi_1), g'(\varphi_2), \cdots, g'(\varphi_K)) \in \mathbb{C}^{K\times K}. \tag{21}$$

Similarly, based on the linear relation between the array steering vectors of sub-arrays X and Z, we can also obtain

$$\boldsymbol{a}'_{z\theta}(\theta_k,\varphi_k) = \boldsymbol{a}'_{x\theta}(\theta_k,\varphi_k)h(\theta_k,\varphi_k) + \boldsymbol{a}_x(\theta_k,\varphi_k)h'_\theta(\theta_k,\varphi_k), \tag{22}$$

$$\boldsymbol{a}'_{z\varphi}(\theta_k,\varphi_k) = \boldsymbol{a}'_{x\varphi}(\theta_k,\varphi_k)h(\theta_k,\varphi_k) + \boldsymbol{a}_x(\theta_k,\varphi_k)h'_\varphi(\theta_k,\varphi_k), \tag{23}$$

where $h'_\theta(\theta_k,\varphi_k)$ and $h'_\varphi(\theta_k,\varphi_k)$ are the first-order partial derivatives of $h(\theta_k,\varphi_k)$ around $\theta = \theta_k$ and $\varphi = \varphi_k$, respectively.

Therefore, from (4), (13), (22) and (23), we can also establish the following generalized rotational invariance relationship as

$$\bar{\boldsymbol{A}}_z = \bar{\boldsymbol{A}}_x \boldsymbol{\Omega}, \tag{24}$$

where

$$\boldsymbol{\Omega} = \begin{bmatrix}\boldsymbol{\Lambda}_{Z1} & \boldsymbol{\Lambda}_{Z2} & \boldsymbol{\Lambda}_{Z3}\\ \boldsymbol{0}_{K\times K} & \boldsymbol{\Lambda}_{Z1} & \boldsymbol{0}_{K\times K}\\ \boldsymbol{0}_{K\times K} & \boldsymbol{0}_{K\times K} & \boldsymbol{\Lambda}_{Z1}\end{bmatrix} \in \mathbb{C}^{3K\times 3K}, \tag{25}$$

in which,

$$\boldsymbol{\Lambda}_{Z1} = diag(h(\theta_1,\varphi_1), h(\theta_2,\varphi_2), \cdots, h(\theta_K,\varphi_K)) \in \mathbb{C}^{K\times K}, \tag{26}$$

$$\boldsymbol{\Lambda}_{Z2} = diag(h'_\theta(\theta_1,\varphi_1), h'_\theta(\theta_2,\varphi_2), \cdots, h'_\theta(\theta_K,\varphi_K)) \in \mathbb{C}^{K\times K}, \tag{27}$$

$$\boldsymbol{\Lambda}_{Z3} = diag(h'_\varphi(\theta_1,\varphi_1), h'_\varphi(\theta_2,\varphi_2), \cdots, h'_\varphi(\theta_K,\varphi_K)) \in \mathbb{C}^{K\times K}. \tag{28}$$

According to (13), (18) and (24), the total array output vector $\boldsymbol{w}(t) \in \mathbb{C}^{3M\times 1}$ can be written as

$$\begin{aligned}\boldsymbol{w}(t) &= \begin{bmatrix}\boldsymbol{w}_z(t)\\ \boldsymbol{w}_y(t)\\ \boldsymbol{w}_x(t)\end{bmatrix} = \begin{bmatrix}\bar{\boldsymbol{A}}_x\boldsymbol{\Omega}\\ \bar{\boldsymbol{A}}_x\boldsymbol{\Phi}\\ \bar{\boldsymbol{A}}_x\end{bmatrix}\bar{\boldsymbol{s}}(t) + \begin{bmatrix}\boldsymbol{n}_z(t)\\ \boldsymbol{n}_y(t)\\ \boldsymbol{n}_x(t)\end{bmatrix}\\ &= \boldsymbol{D}\bar{\boldsymbol{s}}(t) + \boldsymbol{n}(t),\end{aligned} \tag{29}$$

where $\boldsymbol{D} = [(\bar{\boldsymbol{A}}_x\boldsymbol{\Omega})^T, (\bar{\boldsymbol{A}}_x\boldsymbol{\Phi})^T, (\bar{\boldsymbol{A}}_x)^T]^T$ and $\boldsymbol{n}(t) = [\boldsymbol{n}_z(t), \boldsymbol{n}_y(t), \boldsymbol{n}_x(t)]^T$.

In this paper, we consider the case where the received signal is strictly noncircular signal with the maximal noncircularity rate. Thus $\bar{\boldsymbol{s}}(t)$ can be rewritten as (see Appendix)

$$\bar{\boldsymbol{s}}(t) = \boldsymbol{\Xi}\bar{\boldsymbol{s}}_0(t), \tag{30}$$

where $\bar{\boldsymbol{s}}_0(t) \in \mathbb{R}^{3K\times 1}$ is a real-valued signal vector; $\boldsymbol{\Xi} = diag\{e^{j\varpi_1}, , e^{j\varpi_2}, \cdots, e^{j\varpi_{3K}}\}$ is a diagonal matrix of size $3K \times 3K$ containing the rotation phase shifts $\boldsymbol{\varpi} = [\varpi_1, \varpi_2 \cdots, \varpi_{3K}]^T$ on its diagonal.

Exploiting the noncircular property of signal, the extended array output vector $\boldsymbol{w}^{(nc)}(t) \in \mathbb{C}^{6M\times 1}$ of the total array can be written as [18]–[24]

$$\begin{aligned}\boldsymbol{w}^{(nc)}(t) &= \begin{bmatrix}\boldsymbol{w}(t)\\ \boldsymbol{w}^*(t)\end{bmatrix} = \begin{bmatrix}\boldsymbol{D}\\ \boldsymbol{D}^*\boldsymbol{\Xi}^{-2}\end{bmatrix}\bar{\boldsymbol{s}}(t) + \begin{bmatrix}\boldsymbol{n}(t)\\ \boldsymbol{n}^*(t)\end{bmatrix}\\ &= \boldsymbol{D}^{(nc)}\bar{\boldsymbol{s}}(t) + \boldsymbol{n}^{(nc)}(t),\end{aligned} \tag{31}$$

where $\boldsymbol{D}^{(nc)} = [\boldsymbol{D}^T, (\boldsymbol{D}^*\boldsymbol{\Xi}^{-2})^T]^T \in \mathbb{C}^{6M\times 3K}$ is the extended GAM matrix, $\boldsymbol{n}^{(nc)}(t) = [\boldsymbol{n}(t), \boldsymbol{n}^*(t)]^T \in \mathbb{C}^{6M\times 1}$ is the extended received noise vector.

B. AUTO-PAIRING 2-D DOA ESTIMATION ALGORITHM BASED ON THE MODIFIED PM

In this section, we will briefly introduce the computational efficient modified PM for the 2-D DOA estimation of ID noncircular sources, which can also achieve automatic pairing of the estimated parameters.

Since it is assumed that ID sources are mutually uncorrelated, the extended GAM matrix $\boldsymbol{D}^{(nc)} \in \mathbb{C}^{6M\times 3K}$ is of full rank. Thus there are $3K$ rows that are linearly independent in $\boldsymbol{D}^{(nc)}$, and the other rows are the linear representations of them. Assume that the first $3K$ rows of $\boldsymbol{D}^{(nc)}$ are linearly independent, and we partition the matrix $\boldsymbol{D}^{(nc)}$ as

$$\boldsymbol{D}^{(nc)} = [\boldsymbol{D}_1^T, \boldsymbol{D}_2^T]^T, \tag{32}$$

where $\boldsymbol{D}_1$ and $\boldsymbol{D}_2$ are sub-matrices of size $3K \times 3K$ and $(6M - 3K) \times 3K$. Then, a $3K \times (6M - 3K)$ propagator matrix $\boldsymbol{P}$ is defined as a unique linear operator of the form

$$\boldsymbol{P}^H \boldsymbol{D}_1 = \boldsymbol{D}_2. \tag{33}$$

In (33), $\boldsymbol{P}$ can be calculated by the extended array output matrix $\boldsymbol{W}^{(nc)} = [\boldsymbol{w}^{(nc)}(1), \boldsymbol{w}^{(nc)}(2), \cdots, \boldsymbol{w}^{(nc)}(T)]$, where T is the number of snapshots. Partition $\boldsymbol{W}^{(nc)}$ into

$$\boldsymbol{W}^{(nc)} = [(\boldsymbol{W}_1^{(nc)})^T, (\boldsymbol{W}_2^{(nc)})^T]^T, \tag{34}$$

where $\boldsymbol{W}_1^{(nc)} \in \mathbb{C}^{3K\times T}$ and $\boldsymbol{W}_2^{(nc)} \in \mathbb{C}^{(6M-3K)\times T}$. In the noiseless case, $\boldsymbol{W}_2^{(nc)} = \boldsymbol{P}^H \boldsymbol{W}_1^{(nc)}$. However, there is always noise in the practical case, thus the propagator matrix $\boldsymbol{P}$ can be estimated by the least squares approach as

$$\hat{\boldsymbol{P}} = (\boldsymbol{W}_1^{(nc)}(\boldsymbol{W}_1^{(nc)})^H)^{-1} \boldsymbol{W}_1^{(nc)} (\boldsymbol{W}_2^{(nc)})^H. \tag{35}$$

In order to make full use of all array information, an extended propagator matrix $\boldsymbol{P}_e$ can be constructed as $\boldsymbol{P}_e = [\mathbf{I}_{3K}^H, \hat{\boldsymbol{P}}]^H$, and we can have

$$\boldsymbol{P}_e \boldsymbol{D}_1 = \boldsymbol{D}^{(nc)}. \tag{36}$$

We can further partition $\boldsymbol{P}_e$ as

$$\boldsymbol{P}_e = [\boldsymbol{P}_1^T, \boldsymbol{P}_2^T, \boldsymbol{P}_3^T, \boldsymbol{P}_4^T, \boldsymbol{P}_5^T, \boldsymbol{P}_6^T]^T, \tag{37}$$

where $\boldsymbol{P}_1, \boldsymbol{P}_2, \boldsymbol{P}_3, \boldsymbol{P}_4, \boldsymbol{P}_5$ and $\boldsymbol{P}_6$ are all sub-matrices of size $M \times 3K$. Using (29), (31), (36) and (37) produces

$$\begin{bmatrix} \boldsymbol{P}_1 \\ \boldsymbol{P}_2 \\ \boldsymbol{P}_3 \\ \boldsymbol{P}_4 \\ \boldsymbol{P}_5 \\ \boldsymbol{P}_6 \end{bmatrix} \boldsymbol{D}_1 = \begin{bmatrix} \bar{\boldsymbol{A}}_x \boldsymbol{\Omega} \\ \bar{\boldsymbol{A}}_x \boldsymbol{\Phi} \\ \bar{\boldsymbol{A}}_x \\ \bar{\boldsymbol{A}}_x^* \boldsymbol{\Omega}^* \boldsymbol{\Xi}^{-2} \\ \bar{\boldsymbol{A}}_x^* \boldsymbol{\Phi}^* \boldsymbol{\Xi}^{-2} \\ \bar{\boldsymbol{A}}_x^* \boldsymbol{\Xi}^{-2} \end{bmatrix}. \tag{38}$$

By defining the selection matrices

$$\boldsymbol{J}_1 = \begin{bmatrix} \mathbf{0}_{M\times 2M} & \mathbf{I}_M & \mathbf{0}_{M\times 3M} \\ \mathbf{0}_{M\times 4M} & \mathbf{I}_M & \mathbf{0}_{M\times M} \end{bmatrix}, \tag{39}$$

and

$$\boldsymbol{J}_2 = \begin{bmatrix} \mathbf{0}_{M\times M} & \mathbf{I}_M & \mathbf{0}_{M\times 4M} \\ \mathbf{0}_{M\times M} & \mathbf{0}_{M\times 4M} & \mathbf{I}_M \end{bmatrix}, \tag{40}$$

we can obtain

$$\boldsymbol{J}_1 \boldsymbol{P}_e \boldsymbol{D}_1 = \boldsymbol{J}_1 \boldsymbol{D}^{(nc)}, \tag{41}$$

$$\boldsymbol{J}_2 \boldsymbol{P}_e \boldsymbol{D}_1 = \boldsymbol{J}_2 \boldsymbol{D}^{(nc)}. \tag{42}$$

Bringing together (41) and (42) in association with the relation $\boldsymbol{J}_2 \boldsymbol{D}^{(nc)} = \boldsymbol{J}_1 \boldsymbol{D}^{(nc)} \boldsymbol{\Phi}$, we can achieve

$$\boldsymbol{J}_2 \boldsymbol{P}_e \boldsymbol{D}_1 = \boldsymbol{J}_1 \boldsymbol{P}_e \boldsymbol{D}_1 \boldsymbol{\Phi}. \tag{43}$$

From (43), a newly defined matrix $\boldsymbol{\Upsilon} \in \mathbb{C}^{3K\times 3K}$ is presented as follow:

$$\boldsymbol{\Upsilon} = (\boldsymbol{J}_1 \boldsymbol{P}_e)^+ \boldsymbol{J}_2 \boldsymbol{P}_e = \boldsymbol{D}_1 \boldsymbol{\Phi} \boldsymbol{D}_1^{-1}. \tag{44}$$

By performing the EVD on $\boldsymbol{\Upsilon}$, we obtain the diagonal matrix $\hat{\boldsymbol{\Phi}}_1$ consisting of eigenvalues in its principal diagonal and unitary matrix $\hat{\boldsymbol{D}}_1$. The following relationships exist with the matrix $\boldsymbol{D}_1$ and the diagonal matrix $\boldsymbol{\Phi}_1$, whose diagonal elements are the same as those of the upper triangular matrix $\boldsymbol{\Phi}$:

$$\hat{\boldsymbol{\Phi}}_1 = \boldsymbol{\Pi} \boldsymbol{\Phi}_1 \boldsymbol{\Pi}, \tag{45}$$

$$\hat{\boldsymbol{D}}_1 = \boldsymbol{D}_1 \boldsymbol{\Pi}, \tag{46}$$

where $\boldsymbol{\Pi}$ is a permutation matrix with $\boldsymbol{\Pi} = \boldsymbol{\Pi}^{-1}$.

To achieve automatic pairing, we further define the selection matrices as follows:

$$\boldsymbol{J}_3 = \begin{bmatrix} \mathbf{0}_{M\times 2M} & \mathbf{I}_M & \mathbf{0}_{M\times 3M} \\ \mathbf{0}_{M\times 3M} & \mathbf{I}_M & \mathbf{0}_{M\times 2M} \end{bmatrix}, \tag{47}$$

$$\boldsymbol{J}_4 = \begin{bmatrix} \mathbf{I}_M & \mathbf{0}_{M\times 2M} & \mathbf{0}_{M\times 3M} \\ \mathbf{0}_{M\times 2M} & \mathbf{0}_{M\times 3M} & \mathbf{I}_M \end{bmatrix}. \tag{48}$$

Using the estimated extended GAM sub-matrix $\hat{\boldsymbol{D}}_1$, the following two matrices can be constructed:

$$\boldsymbol{E}_1 = \boldsymbol{J}_3 \boldsymbol{P}_e \hat{\boldsymbol{D}}_1, \tag{49}$$

$$\boldsymbol{E}_2 = \boldsymbol{J}_4 \boldsymbol{P}_e \hat{\boldsymbol{D}}_1. \tag{50}$$

Thererfore, according to (38) and (46), the following relationship holds:

$$\boldsymbol{E}_2 = \boldsymbol{E}_1 \hat{\boldsymbol{\Omega}}_1, \tag{51}$$

where $\hat{\boldsymbol{\Omega}}_1 = \boldsymbol{\Pi} \boldsymbol{\Omega}_1 \boldsymbol{\Pi}$, in which $\boldsymbol{\Omega}_1$ is a diagonal matrix whose diagonal elements are the same as those of the upper triangular matrix $\boldsymbol{\Omega}$. Hence, the estimation of the diagonal elements in $\boldsymbol{\Omega}_1$ can be achieved from the diagonal elements of $\boldsymbol{E}_1^+ \boldsymbol{E}_2$.

According to the expressions of the diagonal elements of $\boldsymbol{\Phi}$ and $\boldsymbol{\Omega}$ given in (20) and (26), we can obtain

$$\alpha_{3(k-1)+h} \approx e^{-j2\pi(d/\lambda)\cos\varphi_k} \tag{52}$$

$$\beta_{3(k-1)+w} \approx e^{-j2\pi(d/\lambda)\sin\varphi_k \cos\theta_k} \tag{53}$$

where $k = 1, 2, \cdots, K$; $h = 1, 2, 3$; $\alpha_{3(k-1)+h}$ and $\beta_{3(k-1)+h}$ are the $(3(k-1)+h)$-th diagonal elements of $\hat{\boldsymbol{\Phi}}_1$ and $\hat{\boldsymbol{\Omega}}_1$, respectively. Finally, the estimated central elevation DOA and central azimuth DOA for each source can be expressed as

$$\hat{\varphi}_k = \frac{1}{3}\sum_{h=1}^{3} \arccos\left(-\frac{\lambda \cdot \text{angle}(\alpha_{3(k-1)+h})}{2\pi d}\right), \tag{54}$$

and

$$\hat{\theta}_k = \frac{1}{3}\sum_{h=1}^{3}\arccos\left(-\frac{\lambda\cdot \text{angle}(\beta_{3(k-1)+h})}{\sqrt{(2\pi d/\lambda)^2-(\text{angle}(\alpha_{3(k-1)+h}))^2}}\right). \tag{55}$$

At this point, the estimated central DOAs $\hat{\theta}_k$ and $\hat{\varphi}_k$ have been automatically paired using (54) and (55). The main steps of the proposed algorithm are summarized as follows:

Algorithm 1 Auto-pairing 2-D DOA Estimation Algorithm Based on the Modified PM

Step 1 Construct the extended array output vector $\boldsymbol{w}^{(nc)}(t)$ via (31).
Step 2 Partition the extended array output matrix $\boldsymbol{W}^{(nc)} = [\boldsymbol{w}^{(nc)}(1), \boldsymbol{w}^{(nc)}(2), \cdots, \boldsymbol{w}^{(nc)}(T)]$ to estimate $\hat{\boldsymbol{P}}$ and $\boldsymbol{P}_e$ via (35).
Step 3 Perform the EVD on the constructed matrix $\boldsymbol{\Upsilon}$ with (44) to estimate $\hat{\boldsymbol{\Phi}}_1$ and $\hat{\boldsymbol{D}}_1$.
Step 4 Construct the matrices $\boldsymbol{E}_1$ and $\boldsymbol{E}_2$, and calculate $\hat{\boldsymbol{\Omega}}_1$ via (51).
Step 5 Attain the estimates of $\hat{\varphi}_k$ and $\hat{\theta}_k$ from equations (54) and (55).

IV. ANALYSIS OF THE PROPOSED ALGORITHM

A. COMPLEXITY ANALYSIS

In this section, when the number of total sensor elements M_1, the number of signal sources K and the number of snapshots T change, we analyze the computational complexity of the proposed algorithm in comparison with the algorithms in [15] and [17]. The proposed algorithm does not need spectrum searching, estimation or eigenvalue decomposition of the high-dimensional sample covariance matrix. The main computational cost of the proposed algorithm is mostly made of three operations: the estimation of the propagator $\hat{\boldsymbol{P}}$, the estimation and eigenvalue decomposition of the newly defined matrix $\boldsymbol{\Upsilon}$, and the calculation of the diagonal matrix $\hat{\boldsymbol{\Omega}}_1$, whose corresponding computational complexities are $O(6KM_1\,T+9M_1\,K^2+27K^3)$, $O(9M_1\,K^2+54K^3)$, and $O(9M_1K^2+27K^3)$, respectively. In above, the total computational complexity of the proposed algorithm is $O(6KM_1\,T+27M_1\,K^2+108K^3)$. Moreover, the main computational complexities and the average MATLAB running time[1] of the algorithms in [15] and [17] are given in Table 2 (L denotes the number of searching points). Though the running time cannot rigorously represent the complexity, it more or less provides an intuitive feeling for the complexity comparison among these algorithms. As shown in Table 2, the proposed algorithm provides significantly lower computational cost compared to the other algorithms.

[1]The specific parameters for MATLAB simulations are presented in the second example in Section V: Simulations.

TABLE 2. Complexity comparison.

Algorithm	Complexity	Average Run time(ms)
Proposed	$O(6KM_1T+27M_1K^2+108K^3)$	0.80
ESPRIT+GMUSIC [15]	$O(M_1^2T+M_1^3+27M_1K^2+3M_1KL(M_1-3K)/2+27K^3)$	5266.30
2D-ESPRIT [17]	$O(M_1^2T+M_1^3+36(M_1-1)K^2+108K^3)$	5.64

B. THE CRAMER-RAO LOWER BOUND (CRLB)

The array steering vector of the total array can be rewritten as the following form

$$h(\theta_k,\varphi_k) = \begin{bmatrix} e^{-j(2\pi/\lambda)(p_{x1}\cos\theta_k\sin\varphi_k+p_{y1}\sin\theta_k\sin\varphi_k+p_{z1}\cos\varphi_k)} \\ e^{-j(2\pi/\lambda)(p_{x2}\cos\theta_k\sin\varphi_k+p_{y2}\sin\theta_k\sin\varphi_k+p_{z2}\cos\varphi_k)} \\ \vdots \\ e^{-j(2\pi/\lambda)(p_{xM_1}\cos\theta_k\sin\varphi_k+p_{yM_1}\sin\theta_k\sin\varphi_k+p_{zM_1}\cos\varphi_k)} \end{bmatrix}, \tag{56}$$

where $M_1 = 3M$ is the number of the array sensor elements in the total array, whose m-th element is placed at (p_{xm}, p_{ym}, p_{zm}) for $m = 1, 2, \cdots, M_1$.

Taking advantage of the signal non-circularity, the extended covariance matrix can be written as

$$\boldsymbol{R}^{(nc)} = \begin{bmatrix} \boldsymbol{R} & \boldsymbol{R}_1 \\ \boldsymbol{R}_1^* & \boldsymbol{R}^* \end{bmatrix}, \tag{57}$$

where $\boldsymbol{R}$ and $\boldsymbol{R}_1$ are the conjugated and unconjugated covariance matrix, respectively. According to (1), $\boldsymbol{R}$ is given by [15], [17]

$$\boldsymbol{R} = \sum_{k=1}^{K}\sigma_k^2\,\boldsymbol{\Xi}_k + \sigma_n^2\mathbf{I}_{M_1}, \tag{58}$$

where $\sigma_k^2 = S_k\sigma_{\gamma k}^2$, and $S_k = E[s_k(t)\cdot s_k^*(t)]$ is the signal power of the k-th ID source. Moreover, $\boldsymbol{\Xi}_k$ can be written as

$$\boldsymbol{\Xi}_k = (\boldsymbol{h}(\theta_k,\varphi_k)\boldsymbol{h}^H(\theta_k,\varphi_k))\odot\boldsymbol{T}_k = \boldsymbol{G}_k\boldsymbol{T}_k\boldsymbol{G}_k^H, \tag{59}$$

where $\boldsymbol{G}_k = \text{diag}(\boldsymbol{h}(\theta_k,\varphi_k)) \in \mathbb{C}^{3M\times 3M}$, and each entry of $\boldsymbol{T}_k$ equals (under the assumption that the angular distributed functions are Gaussian function) [17]

$$[\boldsymbol{T}_k]_{m,n} = e^{-\frac{(\mu\sigma_{\theta_k}v_1)^2+(\mu\sigma_{\varphi_k}v_2)^2}{2}}, \tag{60}$$

in which,

$$v_1 = -(p_{xm}-p_{xn})\sin\theta_k\sin\varphi_k + (p_{ym}-p_{yn}) \times\cos\theta_k\sin\varphi_k, \tag{61}$$

$$v_2 = (p_{xm}-p_{xn})\cos\theta_k\cos\varphi_k + (p_{ym}-p_{yn}) \times\sin\theta_k\cos\varphi_k - (p_{zm}-p_{zn})\cos\varphi_k. \tag{62}$$

Similarly, unconjugated covariance matrix $\boldsymbol{R}_1$ can be written as (under the assumption that the noncircular rates are known as 1):

$$\boldsymbol{R}_1 = \sum_{i=1}^{K}\sigma_k^2\beta_k\,\boldsymbol{\Xi}_k', \tag{63}$$

where β_k is the noncircular phase of the k-th ID noncircular source; $\boldsymbol{\Xi}'_k = (\boldsymbol{h}(\theta_k, \varphi_k)\boldsymbol{h}^T(\theta_k, \varphi_k)) \odot \boldsymbol{T}'_k = \boldsymbol{G}_k \boldsymbol{T}'_k \boldsymbol{G}_k^T$, and each entry of $\boldsymbol{T}'_k$ equals

$$[\boldsymbol{T}'_k]_{m,n} = e^{-\frac{(\mu\sigma_{\theta_k} v_3)^2 + (\mu\sigma_{\varphi_k} v_4)^2}{2}}, \tag{64}$$

in which,

$$\begin{aligned} v_3 &= -(p_{xm} + p_{xn}) \sin\theta_k \sin\varphi_k + (p_{ym} + p_{yn}) \\ &\quad \times \cos\theta_k \sin\varphi_k, \end{aligned} \tag{65}$$

$$\begin{aligned} v_4 &= (p_{xm} + p_{xn}) \cos\theta_k \cos\varphi_k + (p_{ym} + p_{yn}) \\ &\quad \times \sin\theta_k \cos\varphi_k - (p_{zm} + p_{zn}) \cos\varphi_k. \end{aligned} \tag{66}$$

To derive the CRLB of the underlying estimation problem, let us define a vector $\boldsymbol{\mu}$ containing all the central DOA parameters as

$$\boldsymbol{\mu} = [\boldsymbol{\mu}_\theta^T, \boldsymbol{\mu}_\varphi^T]^T \in \mathbb{R}^{2K\times 1}, \tag{67}$$

where $\boldsymbol{\mu}_\theta = [\theta_1, \theta_2, \cdots, \theta_K]^T \in \mathbb{R}^{K\times 1}$ and $\boldsymbol{\mu}_\varphi = [\varphi_1, \varphi_2, \ldots, \varphi_K]^T \in \mathbb{R}^{K\times 1}$ containing the center azimuth and elevation DOAs to be estimated, respectively. Next, define a new vector $\boldsymbol{\upsilon}$ containing the other unknown parameters:

$$\boldsymbol{\upsilon} = [\boldsymbol{\mu}_{\sigma_\theta}^T, \boldsymbol{\mu}_{\sigma_\varphi}^T, \boldsymbol{\mu}_\beta^T, \sigma_1^2, \cdots, \sigma_K^2, \sigma_n^2]^T \in \mathbb{R}^{(4K+1)\times 1}, \tag{68}$$

where $\boldsymbol{\mu}_{\sigma_\theta} = [\sigma_{\theta_1}, \sigma_{\theta_2}, \cdots, \sigma_{\theta_K}]^T \in \mathbb{R}^{K\times 1}$ and $\boldsymbol{\mu}_{\sigma_\varphi} = [\sigma_{\varphi_1}, \sigma_{\varphi_2}, \cdots, \sigma_{\varphi_K}]^T \in \mathbb{R}^{K\times 1}$ containing the standard deviations of the azimuth angle spreads and elevation angle spreads, respectively. $\boldsymbol{\mu}_\beta = [\beta_1, \beta_2, \cdots, \beta_K]^T \in \mathbb{R}^{K\times 1}$ containing the noncircular phases.

Then, the vector $\boldsymbol{\varepsilon}$ composed of all the unknown parameters is denoted by

$$\boldsymbol{\varepsilon} = [\boldsymbol{\mu}^T, \boldsymbol{\upsilon}^T]^T \in \mathbb{R}^{(6K+1)\times 1}. \tag{69}$$

The CRLB of $\boldsymbol{\varepsilon}$ can be computed from [26]

$$\text{CRLB}(\boldsymbol{\varepsilon}) = \mathbf{I}_F^{-1}(\boldsymbol{\varepsilon}), \tag{70}$$

where $\mathbf{I}_F(\boldsymbol{\varepsilon})$ is the Fisher information matrix (FIM), whose entries are defined as

$$(\mathbf{I}_F)_{q,q'} = \frac{N}{2} tr((\boldsymbol{R}^{(nc)})^{-1} \frac{\partial \boldsymbol{R}^{(nc)}}{\partial [\boldsymbol{\varepsilon}]_q} (\boldsymbol{R}^{(nc)})^{-1} \frac{\partial \boldsymbol{R}^{(nc)}}{\partial [\boldsymbol{\varepsilon}]_{q'}}), \tag{71}$$

where $q = 1, 2, \cdots, 6K+1$ and $q' = 1, 2, \cdots, 6K+1$.

Furthermore, $\mathbf{I}_F(\boldsymbol{\varepsilon})$ can take the following form

$$\mathbf{I}_F(\boldsymbol{\varepsilon}) = \begin{bmatrix} \mathbf{I}_{F_{\mu,\mu}} & \mathbf{I}_{F_{\mu,\upsilon}}^T \\ \mathbf{I}_{F_{\mu,\upsilon}} & \mathbf{I}_{F_{\upsilon,\upsilon}} \end{bmatrix}, \tag{72}$$

where $\mathbf{I}_{F_{\mu,\mu}} \in \mathbb{R}^{2K\times 2K}$, $\mathbf{I}_{F_{\mu,\upsilon}} \in \mathbb{R}^{(4K+1)\times 2K}$, and $\mathbf{I}_{F_{\upsilon,\upsilon}} \in \mathbb{R}^{(4K+1)\times(4K+1)}$. Finally, we can obtain the following expression for CRLB of the 2-D central DOAs to be estimated for the ID noncircular sources:

$$\text{CRLB}(\boldsymbol{\mu}) = (\mathbf{I}_{F_{\mu,\mu}} - \mathbf{I}_{F_{\mu,\upsilon}} \mathbf{I}_{F_{\upsilon,\upsilon}}^{-1} \mathbf{I}_{F_{\mu,\upsilon}}^T)^{-1}. \tag{73}$$

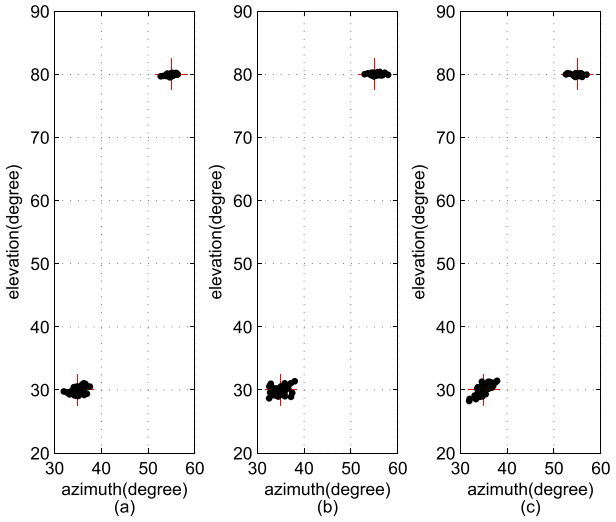

FIGURE 2. The central elevation and azimuth DOAs estimation results (SNR = 5dB). (a), (b) and (c) correspond to three cases: the uniform distributed function, the Gaussian distributed function, and the uniform and Gaussian distributed functions coexist.

V. SIMULATIONS

In this section, the performance of the proposed algorithm is analyzed through simulations. We consider that the involved ID sources emit the BPSK signals impinging on the sensor array as shown in Fig. 1. The noncircular phases set to be random. The variance of ray-gains is set as $\sigma_{\gamma_k}^2 = 1 (k = 1, 2, \cdots, K)$, and the number of scattering paths is set as $L_k = 200 (k = 1, 2, \cdots, K)$. In the following experiments, the number of the whole array sensors is 36, the distance between adjacent sensors in each sub-array is $\lambda/2$, and the distance between sub-arrays is also $\lambda/2$. For simplicity, the k-th ID source is parameterized by the angular parameter vector $\boldsymbol{\mu} = (\theta_k, \sigma_{\theta_k}, \varphi_k, \sigma_{\varphi_k})$, which determines the central azimuth DOA θ_k, the azimuth angular spread parameter σ_{θ_k}, the central elevation DOA φ_k, and the elevation angular spread parameter σ_{φ_k}, respectively. Define the root-mean-square-error (RMSE) of the central azimuth and elevation DOAs respectively as

$$\text{RMSE}(\theta) = \frac{1}{K} \sum_{k=1}^{K} \sqrt{\frac{1}{Q} \left(\sum_{q=1}^{Q} \left\| \hat{\theta}_{k,q} - \theta_k \right\|^2 \right)}, \tag{74}$$

$$\text{RMSE}(\varphi) = \frac{1}{K} \sum_{k=1}^{K} \sqrt{\frac{1}{Q} \left(\sum_{q=1}^{Q} \left\| \hat{\varphi}_{k,q} - \varphi_k \right\|^2 \right)}, \tag{75}$$

where Q is the number of independent Monte-Carlo simulations; $\hat{\theta}_{k,q}$ and $\hat{\varphi}_{k,q}$ are the estimates of the central azimuth and elevation DOAs of the k-th signal in the q-th Monte Carlo simulation, respectively; θ_k and φ_k are the real value of the central azimuth and elevation DOAs of the k-th signal, respectively. All the simulation results are averaged over 500 times independent Monte Carlo simulations.

In the following simulations, the signal power of sources is assumed to be the same. In addition, signal-to-noise

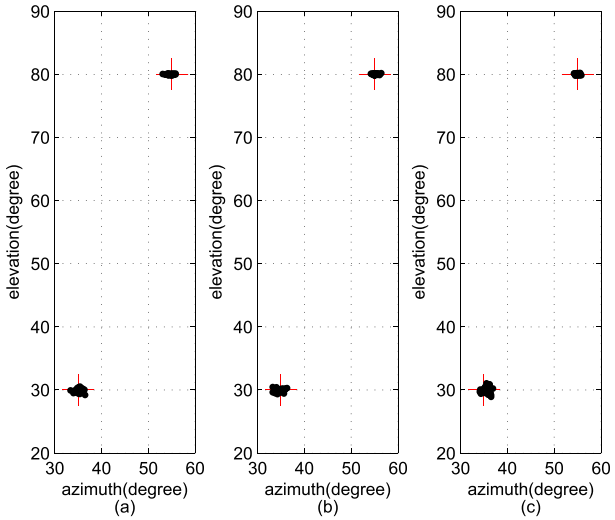

FIGURE 3. The central elevation and azimuth DOAs estimation results (SNR = 15dB). (a), (b) and (c) correspond to three cases: the uniform distributed function, the Gaussian distributed function, and the uniform and Gaussian distributed functions coexist.

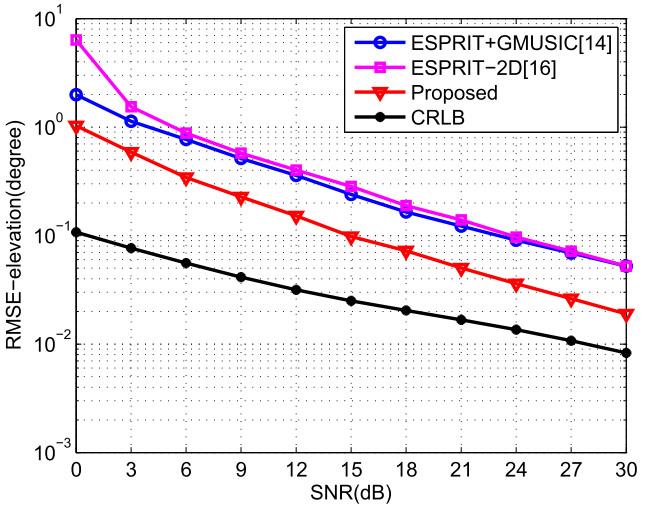

FIGURE 4. RMSEs versus SNR for central elevation DOA estimation.

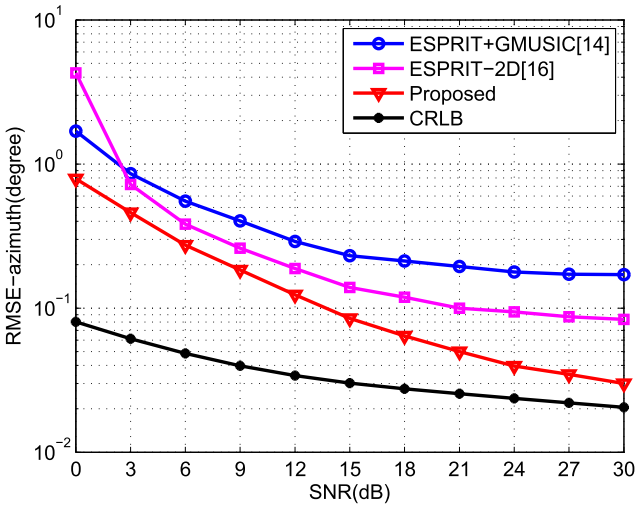

FIGURE 5. RMSEs versus SNR for central azimuth DOA estimation.

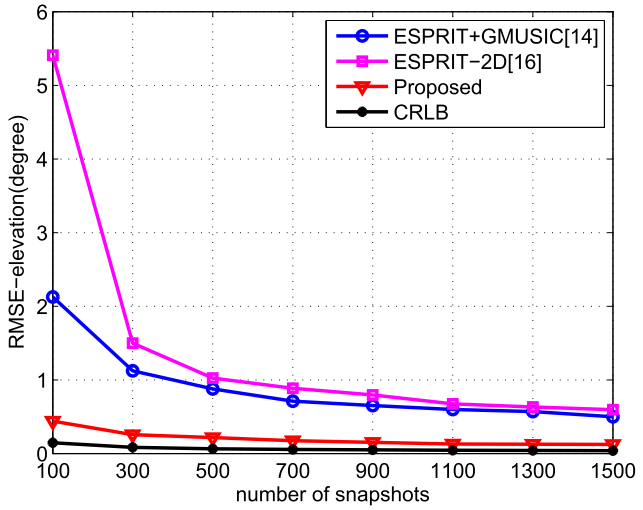

FIGURE 6. RMSEs versus the number of snapshots for central elevation DOA estimation.

ratio (SNR) is defined as

$$\mathrm{SNR} = 10\log\frac{\sigma_s^2}{\sigma_n^2}, \tag{76}$$

where σ_s^2 is the signal power of sources, while σ_n^2 is the variance of noise.

In the first experiment, we investigate if the proposed algorithm works properly for different angular distributed functions. Consider two ID noncircular sources, whose angular parameters are $\boldsymbol{\mu}_1 = (35°, 2°, 30°, 3°)$ and $\boldsymbol{\mu}_2 = (65°, 3°, 80°, 2°)$. The number of snapshots is set as $T = 500$. We perform the algorithm in three cases: 1)the two sources exhibit both uniform distribution; 2)the two sources exhibit both Gaussian distribution; 3)the first source exhibits uniform distribution whereas the second source exhibits Gaussian distribution. The SNR is equal to 5dB. For 50 independent trials, the central DOA estimates of ID sources are plotted in Fig. 2. Similarly, when SNR is equal to 15dB, the central DOA estimates of ID sources are plotted in Fig. 3 (Note that (a), (b) and (c) in Fig. 2 and Fig. 3 correspond to the three cases mentioned above, respectively). It can be seen that the proposed algorithm can give the correct DOA estimates under the case where different ID sources may have different deterministic angular distributed functions. As expected, the error of parameter estimation decreases gradually with the increase of SNR.

In the second experiment, we compare the proposed algorithm with the algorithms in [15] and [17] in respect to estimation performance. In addition, the CRLB is also displayed as a benchmark. The number of snapshots is $N = 500$. The arrays in these algorithms are all composed of 36 sensors. The angular parameters of two Gaussian-shaped ID sources are $\boldsymbol{\mu}_1 = (45°, 1°, 60°, 1.5°)$ and $\boldsymbol{\mu}_2 = (55°, 1.5°, 70°, 1°)$, respectively. The RMSEs of the central elevation DOA

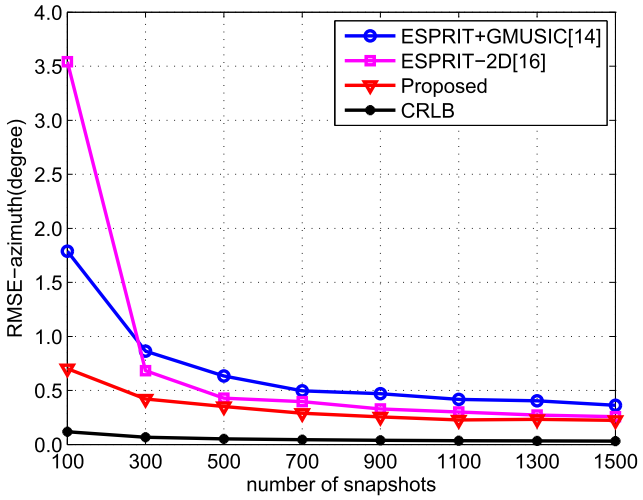

FIGURE 7. RMSEs versus the number of snapshots for central azimuth DOA estimation.

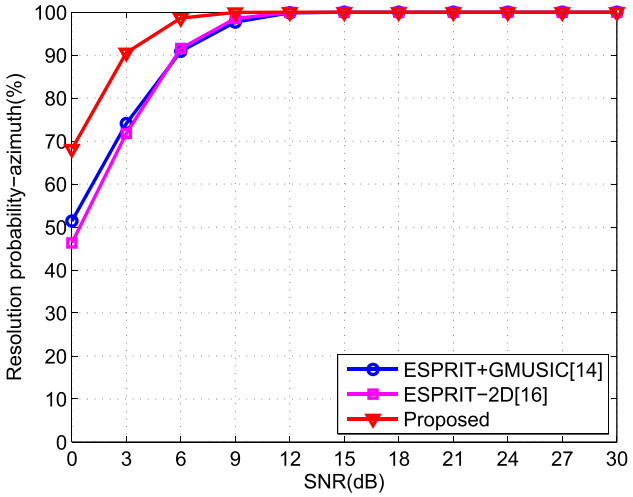

FIGURE 9. Resolution probability versus SNR for central azimuth DOA estimation.

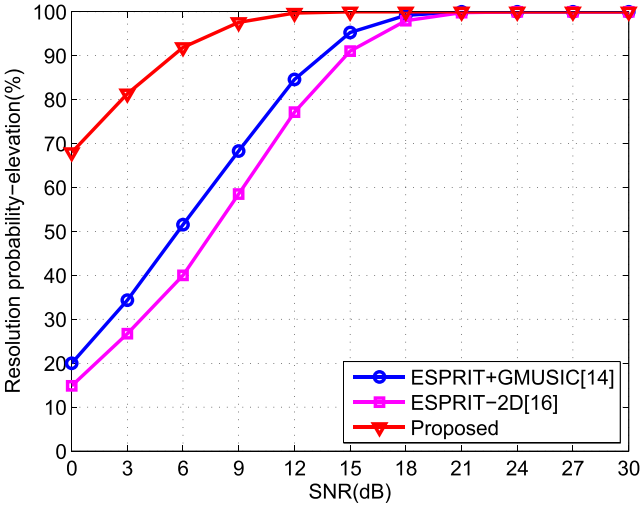

FIGURE 8. Resolution probability versus SNR for central elevation DOA estimation.

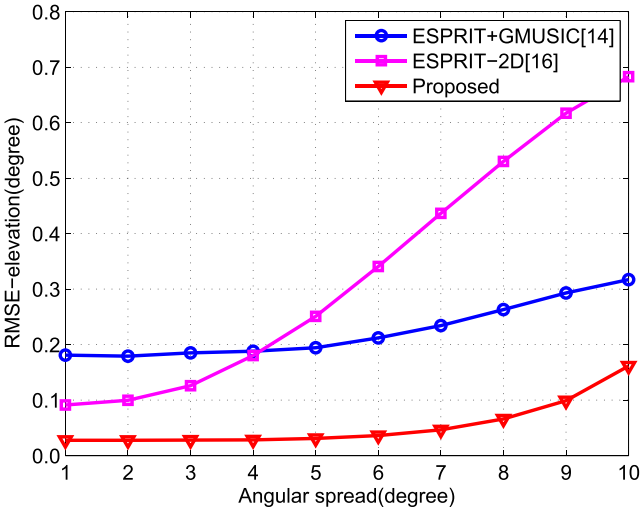

FIGURE 10. RMSEs versus angular spread for central elevation DOA estimation.

estimation and central azimuth DOA estimation versus SNR are shown in Fig. 4 and Fig. 5, respectively. It can be seen that the proposed algorithm has better estimation accuracy compared with the other algorithms, which arises from the fact that the proposed algorithm exploits the noncircular property to improve the performance and does not suffer additional errors brought about by parameter pairing.

In the third experiment, we illustrate the influence of the number of snapshots on the performance of the proposed algorithm. The number of snapshots varies from 100 to 1500. We set SNR = 5dB and the other parameters are the same as the second experiment. The RMSEs of the central elevation DOA estimation and central azimuth DOA estimation for different algorithms are shown in Fig. 6 and Fig. 7, respectively. It is indicated that the estimation performance of the proposed algorithm becomes better in collaboration with the number of snapshots increasing and outperforms other algorithms.

In the fourth experiment, we illustrate the resolution probability versus SNR when two ID noncircular sources are closely spaced (10° separation). The angular parameters of the two Gaussian-shaped ID noncircular sources are $\boldsymbol{\mu}_1 = (30°, 2°, 60°, 3°)$ and $\boldsymbol{\mu}_2 = (40°, 3°, 70°, 2°)$, respectively. As shown in Fig. 8 and Fig. 9, the resolution performance of the proposed algorithm outperforms other algorithms.

In the last experiment, we present the estimation performance of the proposed algorithm compared with other algorithms versus the angular spread in Fig. 10 and Fig. 11. The angular spread varies from 1° to 10°. We set SNR = 20dB and the angular distribution is Gaussian. The other parameters are the same as the second experiment. From Fig. 10 and Fig. 11, it can be observed that with the increase of the angular spread, the estimation performance of the three algorithms deteriorates generally since the Taylor series becomes less accurate when the angular spreads are large.

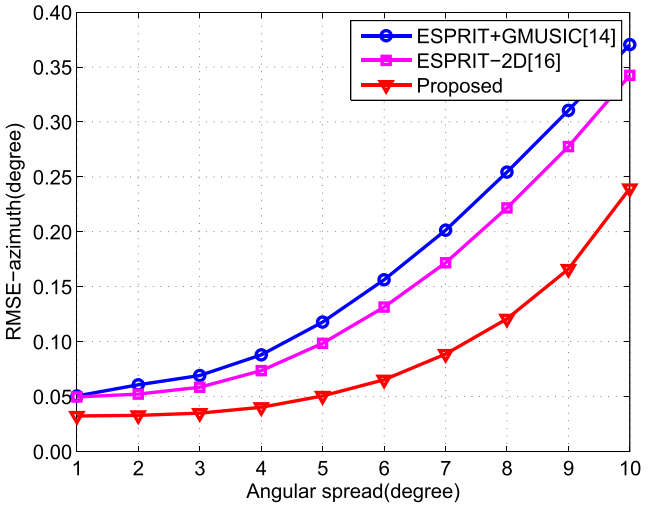

FIGURE 11. RMSEs versus angular spread for central azimuth DOA estimation.

VI. CONCLUSION

In this paper, we developed a 2-D central DOA estimation algorithm for multiple ID noncircular sources with the three-parallel ULAs. Based on the signal non-circularity and Taylor series approximation, we have obtained the generalized rotational invariance relationships among the extended GAMs of the three ULAs. And then the 2-D central DOAs could be obtained by using modified PM. Without spectrum searching, estimation or eigenvalue decomposition of the sample covariance matrix, the proposed algorithm evidently reduces computational cost and is hence suited for real-time processing. Furthermore, the estimated 2-D DOAs are paired automatically. In addition, the proposed method owns better estimation performance and can be applied in the multisource scenario where different sources may have different angular distribution shapes.

APPENDIX

For noncircular signal $s_k\ (t)(k = 1, 2, \cdots, K)$, it holds that [18]–[22]

$$E[s_k(t) \cdot s_k(t)] = \rho_k e^{j\beta_k} E[s_i(t) \cdot s_k^*(t)] \neq 0, \tag{77}$$

where ρ_k and β_k are the noncircular phase and rate of the k-th source, respectively. $\rho = 1$ and $0 \leq \rho \leq 1$ stand for the maximal and common noncircular rated signal, respectively. In this paper, we consider the case where the received signal is strictly noncircular signal with the maximal noncircular rate. Thus the signal vectors $\boldsymbol{s}(t) = [s_1(t), s_2(t), \cdots, s_K(t)]^T$ can be expressed as

$$\boldsymbol{s}(t) = \boldsymbol{\Psi}\boldsymbol{s}_0(t), \tag{78}$$

where $\boldsymbol{s}_0(t) \in \mathbb{R}^{K\times 1}$ is a real-valued vector; $\boldsymbol{\Psi} = \text{diag}\{e^{j\beta_1/2}, e^{j\beta_2/2}, \cdots, e^{j\beta_K/2}\}$ is a diagonal matrix of size $K \times K$; β_k is the noncircular phase of the k-th source.

Define the variables $c_{k,1}$, $c_{k,2}$ and $c_{k,3}$ as

$$\begin{aligned} c_{k,1} &= \sum_{l=1}^{L_k} \gamma_{k,l}(t), \\ c_{k,2} &= \sum_{l=1}^{L_k} \gamma_{k,l}(t)(\theta_{k,l} - \theta_k), \\ c_{k,3} &= \sum_{l=1}^{L_k} \gamma_{k,l}(t)(\varphi_{k,l} - \varphi_k). \end{aligned} \tag{79}$$

Furthermore, according to (12), (15), (78) and (79), $\bar{\boldsymbol{s}}(t)$ can be rewritten as

$$\bar{\boldsymbol{s}}(t) = \boldsymbol{\Gamma}\boldsymbol{s}_1(t) = \boldsymbol{\Gamma}\boldsymbol{\Psi}_1\boldsymbol{s}_{01}(t), \tag{80}$$

in which,

$$\begin{aligned} \boldsymbol{\Gamma} &= \text{diag}(c_{1,1}, \cdots, c_{K,1}, c_{1,2}, \cdots, \\ &\quad c_{K,2}, c_{1,3}, \cdots, c_{K,3}) \in \mathbb{C}^{3K\times 3K}, && (81) \\ \boldsymbol{s}_1(t) &= [(\boldsymbol{s}(t))^T, (\boldsymbol{s}(t))^T, (\boldsymbol{s}(t))^T]^T \in \mathbb{C}^{3K\times 1}, && (82) \\ \boldsymbol{\Psi}_1 &= \text{diag}\{e^{j\beta_1/2}, \cdots, e^{j\beta_K/2}, e^{j\beta_1/2}, \cdots, \\ &\quad e^{j\beta_K/2}, e^{j\beta_1/2}, \cdots, e^{j\beta_K/2}\} \in \mathbb{C}^{3K\times 3K}, && (83) \\ \boldsymbol{s}_{01}(t) &= [(\boldsymbol{s}_0(t))^T, (\boldsymbol{s}_0(t))^T, (\boldsymbol{s}_0(t))^T]^T \in \mathbb{R}^{3K\times 1}. && (84) \end{aligned}$$

According to (7), the path gains $\gamma_{k,l}(t)$ of different paths are uncorrelated. Moreover, $c_{k,1}$ is usually scaled to be 1; $c_{k,2}$ and $c_{k,3}$ are complex-valued. Here, $c_{k,2}$ and $c_{k,3}$ contain the information of the azimuth angle spread and elevation angle spread of k-th ID sources. Thus, we can have

$$\begin{aligned} c_{k,1} &= 1, \\ c_{k,2} &= \left|c_{k,2}\right| e^{jangle(c_{k,2})}, \\ c_{k,3} &= \left|c_{k,3}\right| e^{jangle(c_{k,3})}. \end{aligned} \tag{85}$$

Combine (80) and (85), $\bar{\boldsymbol{s}}(t)$ can be rewritten as

$$\bar{\boldsymbol{s}}(t) = \boldsymbol{\Gamma}_1\boldsymbol{\Gamma}_2\boldsymbol{\Psi}_1\boldsymbol{s}_{01}(t), \tag{86}$$

where

$$\begin{aligned} \boldsymbol{\Gamma}_1 &= \text{diag}(1, \cdots, 1, e^{jangle(c_{1,2})}, \cdots, e^{jangle(c_{K,2})}, \\ &\quad \times e^{jangle(c_{1,3})}, \cdots, e^{jangle(c_{K,3})}) \in \mathbb{C}^{3K\times 3K}, && (87) \\ \boldsymbol{\Gamma}_2 &= \text{diag}(1, \cdots, 1, \left|c_{1,2}\right|, \cdots, \left|c_{K,2}\right|, \\ &\quad \times \left|c_{1,3}\right|, \cdots, \left|c_{K,3}\right|) \in \mathbb{C}^{3K\times 3K}. && (88) \end{aligned}$$

Finally, $\bar{\boldsymbol{s}}(t)$ can be expressed as

$$\bar{\boldsymbol{s}}(t) = \boldsymbol{\Xi}\bar{\boldsymbol{s}}_0(t), \tag{89}$$

where $\boldsymbol{\Xi} = \boldsymbol{\Gamma}_1\boldsymbol{\Psi}_1 = diag\{e^{j\varpi_1}, , e^{j\varpi_2}, \cdots, e^{j\varpi_{3K}}\}$ is a diagonal matrix of size $3K \times 3K$; $\varpi_k = \eta_k + \mu_k (k = 1, 2, \cdots, 3K)$, η_k and μ_k are the amplitude values of k-th diagonal elements of $\boldsymbol{\Gamma}_1$ and $\boldsymbol{\Psi}_1$, respectively. $\bar{\boldsymbol{s}}_0(t) = \boldsymbol{\Gamma}_2\boldsymbol{s}_{01}(t)$ is a real-value signal vector of size $3K \times 1$.

REFERENCES

[1] H. Krim and M. Viberg, "Two decades of array signal processing research: The parametric approach," *IEEE Signal Process. Mag.*, vol. 13, no. 4, pp. 67–94, Jul. 1996.

[2] F. Yan, M. Jin, and X. Qiao, "Low-complexity DOA estimation based on compressed MUSIC and its performance analysis," *IEEE Trans. Signal Process.*, vol. 61, no. 8, pp. 1915–1930, Apr. 2013.

[3] X. Y. Lan, Y. F. Li, and E. S. Wang, "A rare algorithm for 2D DOA estimation based on nested array in massive mimo system," *IEEE Access*, vol. 4, no. 1, pp. 3806–3814, 2016.

[4] Y. Zhang, X. Xu, Y. A. Sheikh, and Z. Ye, "A rank-reduction based 2-D DOA estimation algorithm for three parallel uniform linear arrays," *Signal Process.*, vol. 120, pp. 305–310, Mar. 2016.

[5] S. Valaee, B. Champagne, and P. Kabal, "Parametric localization of distributed sources," *IEEE Trans. Signal Process.*, vol. 43, no. 9, pp. 2144–2153, Sep. 1995.

[6] O. Besson and P. Stoica, "Decoupled estimation of DOA and angular spread for a spatially distributed source," *IEEE Trans. Signal Process.*, vol. 48, no. 7, pp. 1872–1882, Jul. 2000.

[7] W. Xiong, J. Picheral, and S. Marcos, "Array geometry impact on music in the presence of spatially distributed sources," *Digit. Signal Process.*, vol. 63, pp. 155–163, Apr. 2017.

[8] Y. Meng, P. Stoica, and K. M. Wong, "Estimation of the directions of arrival of spatially dispersed signals in array processing," *IEE Proc.-Radar Sonar Navigat.*, vol. 143, no. 1, pp. 1–9, Feb. 1996.

[9] S. Shahbazpanahi, S. Valaee, and M. H. Bastani, "Distributed source localization using ESPRIT algorithm," *IEEE Trans. Signal Process.*, vol. 49, no. 10, pp. 2169–2178, Oct. 2001.

[10] O. Besson and P. Stoica, "Computationally efficient maximum likelihood approach to DOA estimation of a scattered source," *Wireless Pers. Commun.*, vol. 16, no. 2, pp. 135–148, 2001.

[11] B. T. Sieskul, "An asymptotic maximum likelihood for joint estimation of nominal angles and angular spreads of multiple spatially distributed sources," *IEEE Trans. Veh. Technol.*, vol. 59, no. 3, pp. 1534–1538, Mar. 2010.

[12] S. Shahbazpanahi, S. Valaee, and A. B. Gershman, "A covariance fitting approach to parametric localization of multiple incoherently distributed sources," *IEEE Trans. Signal Process.*, vol. 52, no. 3, pp. 592–600, Mar. 2004.

[13] J. Lee, J. Joung, and J. D. Kim, "A method for the direction-of-arrival estimation of incoherently distributed sources," *IEEE Trans. Veh. Technol.*, vol. 57, no. 5, pp. 2885–2893, Sep. 2008.

[14] H. Boujemaa, "Extension of COMET algorithm to multiple diffuse source localization in azimuth and elevation," *Eur. Trans. Telecommun.*, vol. 16, no. 6, pp. 557–566, 2005.

[15] X. Guo, Q. Wan, X. Shen, and H. Dou, "Low-complexity parameters estimator for multiple 2D domain incoherently distributed sources," *Turkish J. Electr. Eng., Comput. Sci.*, vol. 19, no. 3, pp. 445–462, 2011.

[16] J. Zhou, Z. Zheng, and G. J. Li, "Low-Complexity estimation of the nominal azimuth and elevation for incoherently distributed sources," *Wireless Pers. Commun.*, vol. 71, no. 3, pp. 1777–1793, 2013.

[17] A. Hu, T. Lv, H. Gao, Z. Zhang, and S. Yang, "An ESPRIT-based approach for 2-D localization of incoherently distributed sources in massive MIMO systems," *IEEE J. Sel. Topics Signal Process.*, vol. 8, no. 5, pp. 996–1011, Oct. 2014.

[18] H. Abeida and J.-P. Delmas, "MUSIC-like estimation of direction of arrival for noncircular sources," *IEEE Trans. Signal Process.*, vol. 54, no. 7, pp. 2678–2690, Jul. 2006.

[19] Y. Shi, L. Huang, C. Qian, and H. C. So, "Direction-of-arrival estimation for noncircular sources via structured least squares-based esprit using three-axis crossed array," *IEEE Trans. Aerosp. Electron. Syst.*, vol. 51, no. 2, pp. 1267–1278, Apr. 2015.

[20] G. Zheng, J. Tang, and X. Yang, "Esprit and unitary esprit algorithms for coexistence of circular and noncircular signals in bistatic MIMO radar," *IEEE Access*, vol. 4, no. 99, pp. 7232–7240, 2016.

[21] X. M. Yang, G. J. Li, Z. Zheng, and L. Zhong, "2D DOA estimation of coherently distributed noncircular sources," *Wireless Pers. Commun.*, vol. 78, no. 2, pp. 1095–1102, 2014.

[22] L. T. Wan, G. J. Han, J. F. Jiang, and T. Zhu, "DOA estimation for coherently distributed sources considering circular and noncircular signals in massive MIMO systems," *IEEE Syst. J.*, vol. 11, no. 1, pp. 41–49, Mar. 2017.

[23] X. Yang, G. Li, C. C. Ko, Z. Zheng, and T. S. Yeo, "Central DOA estimation of incoherently distributed noncircular sources with cross-correlation matrix," *Circuits, Syst., Signal Process.*, vol. 34, no. 11, pp. 3697–3707, 2015.

[24] X. Yang, Z. Zheng, and B. Hu, "Off-grid DOA estimation of incoherently distributed non-circular sources via generalised approximate message passing," *Electron. Lett.*, vol. 52, no. 4, pp. 262–264, Jan. 2016.

[25] K. I. Pedersen, P. E. Mogensen, and B. H. Fleury, "Spatial channel characteristics in outdoor environments and their impact on BS antenna system performance," in *Proc. IEEE Veh. Technol. Conf.*, May 2002, pp. 719–723.

[26] M. Kleinsteuber and A. K. Seghouane, "On the deterministic CRB for DOA estimation in unknown noise fields using sparse sensor arrays," *IEEE Trans. Signal Process.*, vol. 56, no. 2, pp. 860–864, Feb. 2008.

ZHENGLIANG DAI received the B.S. degree from the National Digital Switching System Engineering and Technological Research Center, Zhengzhou, China, in 2015, where he is currently pursuing the M.S. degree in communications and information system. His main research interests are in the areas of wireless communication theory, signal processing, and distributed source signal processing.

BIN BA received the M.S. and Ph.D. degrees from the National Digital Switching System Engineering and Technological Research Center (NDSC), Zhengzhou, China, in 2012 and 2015, respectively. He is currently with NDSC in communications and information system. His main research interests are in the areas of wireless communication theory, signal processing, and parameter estimation.

WEIJIA CUI received the M.S. and Ph.D. degrees from the National Digital Switching System Engineering and Technological Research Center (NDSC), Zhengzhou, China, in 2001 and 2007, respectively. He is currently with NDSC in communications and information system. His main research interests are in the areas of wireless communication theory, satellite and mobile communication, and signal processing.

YOUMING SUN received the B.S. degree in electronic and information engineering from Yanshan University, Qinhuangdao, China, in 2010, and the M.S. and Ph.D. degrees from the National Digital Switching System Engineering and Technological Research Center, Zhengzhou, China, in 2013 and 2016, respectively. His research interests include resource allocation in small cell networks, cognitive radio networks, game theory, and statistical learning. He has acted as a Technical Program Committee Member of the IEEE International Conference on Wireless Communications and Signal Processing 2015. He currently a Regular Reviewer for many technical journals, including the IEEE JOURNAL ON SELECTED AREAS IN COMMUNICATIONS, the IEEE TRANSACTIONS ON VEHICULAR TECHNOLOGY, the IEEE SYSTEMS JOURNAL, the IEEE ACCESS, the IEEE COMMUNICATIONS LETTERS, the *Transactions on Emerging Telecommunications Technologies*, and the *IET Communications*.